Surface Engineering

ISSN: 0267-0844 (Print) 1743-2944 (Online) Journal homepage: http://www.tandfonline.com/loi/ysue20

On structure and oxidation behaviour of non-stoichiometric amorphous aluminium phosphate coating

F. S. Sayyedan & M. H. Enayati

To cite this article: F. S. Sayyedan & M. H. Enayati (2019): On structure and oxidation behaviour of non-stoichiometric amorphous aluminium phosphate coating, Surface Engineering

To link to this article: https://doi.org/10.1080/02670844.2018.1560912

Published online: 07 Jan 2019.

SURFACE ENGINEERING
https://doi.org/10.1080/02670844.2018.1560912

The Institute of Materials, Minerals and Mining

Taylor & Francis
Taylor & Francis Group

On structure and oxidation behaviour of non-stoichiometric amorphous aluminium phosphate coating

F. S. Sayyedan and M. H. Enayati

Department of Materials Engineering, Isfahan University of Technology, Isfahan, Iran

ABSTRACT

The purpose of this study was to investigate the structure and oxidation behaviour of non-stoichiometric aluminium phosphate coating. Phase composition analysis was performed by X-ray diffractometer (XRD). Fourier transform infrared (FTIR) was used for molecular spectroscopy. The micro-structural studies were investigated by TEM. AISI 304 stainless steel substrates were dip coated in the aluminium phosphate solution to evaluate the cyclic oxidation behaviour. The oxidised samples were characterised by SEM/EDS and XRD techniques. The XRD patterns and TEM images confirmed the amorphous structure of as-synthesised aluminium phosphate. Based on the FTIR result, the non-stoichiometric amorphous aluminium phosphate owned Al–O–Al bonding besides Al–O–P. Weight change measurements after 100 h oxidation at 1100°C revealed that the range of the weight gain of the bare substrate was 30 times higher than that of the coated one.

ARTICLE HISTORY
Received 1 October 2018
Revised 14 November 2018
Accepted 16 December 2018

KEYWORDS
Aluminium phosphate; amorphous coating; sol-gel; oxidation resistance

Introduction

Aluminium phosphate with chemical composition of $AlPO_4$ is a well-known ceramic material with low density (2.56 g cm^{-3} for berlinite), high melting temperature (1800°C), and high hardness (6.5 Mohs) [1]. It is also chemically compatible with most widely used ceramic materials including silicon carbide, alumina, mullite, and silica over a moderate range of temperatures [2]. However, stoichiometric aluminium phosphate is isostructural with silica and undergoes similar polymorphic transformations (quartz-type, tridymite, and cristobalite). In fact, its use as a high temperature 'engineering ceramic' material is limited primarily because of the phase transformations which involve large molar volume changes [3]. Therefore, synthesis of non-stoichiometric and amorphous aluminium phosphate with no allotropic volume changes which is stable at the elevated temperatures appears advantageous as it skips the aforementioned drawbacks and provides unique properties arising from the amorphous structure such as superior corrosion and oxidation resistance [4].

Non-crystalline aluminophosphates can be prepared at low temperatures by a variety of synthesis procedures common for the route [5–8]. However, all of these amorphous materials crystallise up to 1000°C and forming thermodynamically stable cristobalite $AlPO_4$ and α-Al_2O_3. For instance, Campelo et al. [7] have synthesised amorphous aluminium phosphate using ammonium dihydrogen phosphate ($NH_4H_2PO_4$- which started to crystallise at 800°C. Liu et al. [8] syn- ,) thesised aluminium phosphate from precursors of Al $(NO_3)_3/H_3PO_4/NH_4OH$ in the presence of citric acid which remained amorphous up to 900°C.

The solution-based synthesis of amorphous oxide materials owns advantageous over other processes because glasses can be formed at lower temperatures by atomic or molecular level mixing of the multi-components in a solution [9]. Using the sol-gel process with controlled stoichiometry, the structure remains metastable and overcomes the limitation of thermal stability below 1000°C [1]. Moreover, the crystallisation will be postponed up to higher temperatures or longer times. The sol-gel technique offers the ability to tailor the chemistry at the molecular level, thus novel materials can be produced with unique properties [9].

The purpose of the present research is to synthesise a non-stoichiometric aluminium phosphate coating and to investigate its microstructure and oxidation behaviour.

Materials and methods

Non-stoichiometric amorphous aluminium phosphate synthesis

Non-stoichiometric amorphous aluminium phosphate precursor solution was synthesised by the sol-gel process. Aluminium nitrate nonahydrate ($Al(NO_3)_3.9H_2$-O, Merck, 98.5% purity), phosphorus pentoxide (P_2O_5, Merck, 98% purity), and ethanol (C_2H_5OH, Merck, 99.8% purity) were the starting materials. To synthesise the precursor solution, a certain amount of

CONTACT F.S. Sayyedan fs.sayyedan@ma.iut.ac.ir Department of Materials Engineering, Isfahan University of Technology, Isfahan 84156-83111, Iran

Table 1. Chemical composition of substrate in terms of weight per cent of the elements.

Element	Fe	C	Si	S	P	Mn	Ni	Cr	Mo	Cu	Nb	Ti	V
Wt-%	remain	0.0455	0.295	<0.030	<0.007	1.52	11.3	16.0	<0.050	0.164	0.0705	0.0145	0.0537

$Al(NO_3)_3.9H_2O$ and P_2O_5 were dissolved in ethanol to achieve Al:P = 1.75:1 molar ratio. The two solutions were mixed together homogeneously under constant stirring for 2 h using a magnetic stirrer and allowed to age at room temperature for 24 h. The prepared gel was dried in an oven at 150°C in the air for enough time to complete the dehydration process. This changes the gel into a voluminous, light yellow, and fluffy material. The dried gel was calcined in an electrical furnace in the air at two different temperatures, namely 500°C for 15 min and 1100°C for 1 h, and collected at the end of treatment for subsequent characterisation.

Coating procedure

A 1 mm thick AISI 304 stainless steel sheet was cut into samples of 20×20 mm^2 using a spark wire machine. The chemical composition of the steel substrate is given in Table 1. The samples were ground to 4000 grit SiC abrasive paper followed by polishing using 0.3 µm alumina slurry. The samples were then degreased ultrasonically in acetone, ethanol, and distilled water for 10 min. The prepared solution (according to Section 'Non-stoichiometric amorphous aluminium phosphate synthesis'1) was applied on AISI 304 stainless steel substrates by a dip coater at the constant withdrawal rate of 15 mm min^{-1}. The coated samples were dried in an oven at 150°C and then annealed in the air at 500°C for 15 min.

X-ray diffractometer analysis

Phase composition analysis of the synthesised powder was performed by an X-ray diffractometer (XRD, Philips PW1830) using Ni filtered Cu Ka radiation (lCu Ka = 0.154 nm, radiation at 40 kV and 40 mA) over the 2θ range of 10–70° (time per step: 1.25 s and step size: 0.051°). XRD spectra were compared to standards compiled by the International Centre for Diffraction Data (ICDD).

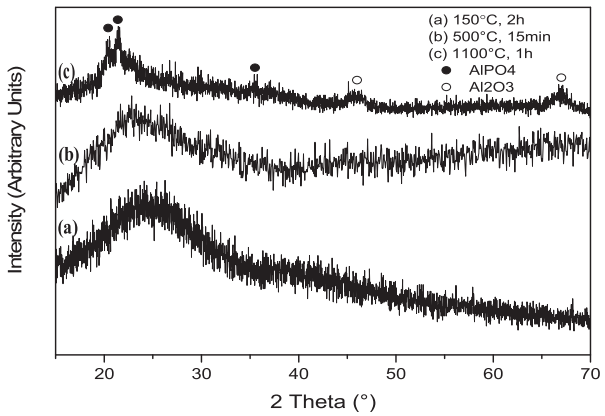

Figure 1. XRD patterns of the synthesised aluminium phosphate (a) gel dried at 150°C for 2 h and powder annealed at (b) 500°C for 15 min and (c) 1100°C for 1 h.

TEM studies

The micro structure of the synthesised powder was studied by TEM (Philips-CM200 FE) technique. The powder sample for TEM observation was prepared by dispersing the powder in methanol and adding a few drops of the suspension on carbon-coated TEM grid.

Fourier transform infrared investigations

The investigation of bonding agents in the synthesised aluminium phosphate was performed by Fourier transform infrared (FTIR) spectroscopy (Bomem, MB 100). The spectrum was recorded in the 4000–400 cm^{-1} range with 2 cm^{-1} resolution.

Cyclic oxidation test

Oxidation behaviour of the coated substrates was evaluated in an electrical furnace at 1100°C for 100 h in the air by weight measurements performed at regular ten-hour intervals. The weight changes of three samples of each thermal cycle were measured by an electrical balance with a sensitivity of ±0.1 mg. The weight gain per unit area ($\Delta W/A$, mg cm^{-2}) was calculated by the equation:

$$\frac{\Delta W}{A} = \frac{W_i - W_0}{A} \quad (1)$$

where W_i (mg) was the weight of the sample after each cycle, W_0 (mg) was the initial weight of the sample before oxidation test, and A (cm^2) was the surface area of the specimen exposed to oxidising atmosphere.

The cross-section and surface of the oxidised samples were characterised by scanning electron microscopy (SEM, Zeiss EVO 50 EP) equipped with energy dispersive X-ray spectrometer (EDS), and an XRD (Philips PW1830).

Results and discussion

Phase composition analysis

The XRD patterns of the synthesised aluminium phosphate powder after drying and different annealing steps

are shown in Figure 1. The dried gel at 150°C does not show any crystalline features and is characterised by a broad hump at low 2θs (between 20° and 30°), indicative of fully amorphous nature. Whereas annealing at 500°C does not remarkably modify the amorphous pattern, the annealing at 1100°C, however, clearly promotes the crystallisation of the coating as demonstrated by the appearance of $AlPO_4$ (ICDD Card No. 003-025-0581) and Al_2O_3 (ICDD Card No. 00-005-0712) crystalline peaks, supposedly embedded in the parent amorphous aluminium phosphate matrix. However, the presence of initial hump at low 2θs along with the low intensity crystalline peaks suggests a mixed amorphous-nanocrystalline structure. This structure was further confirmed by TEM observations presented in the next section.

Micro-structural observations

TEM bright field images and selected area electron diffraction (SAED) patterns of aluminium phosphate gel annealed at different temperatures are shown in Figure 2. The dried gel is composed of micrometer scale particles (Figure 2(a)) with indistinct edges, suggesting insufficiency of drying treatment for any crystalline phase formation. High resolution TEM (HRTEM) image of this sample (Figure 2(b)) confirms lack of crystallinity revealed by the absence of atomic fringes, though demonstrates the presence of smaller constituents, supposedly, aggregated products of sol-gel, in the big particles. The SAED image of this sample (Figure 2(c)) does not show crystalline rings or spots, once more confirming the amorphous nature of the product in agreement with HRTEM (Figure 2(b)) and XRD (Figure 1(a)) results. The indistinct intensity variation in SAED of this sample showing a halo-like feature hardly corresponds to any crystalline plane of expectable materials. The annealed sample at 500° C, in contrast to the dried gel, shows clear and distinct particles (Figure 2(d)) with almost the same size as the dried gel. Annealing has decomposed volatile residues of the gel such as nitrates and organics that leads to clear observation of the constituent particles. Nevertheless, the HRTEM image of this sample (Figure 2 (e)) as well as its SAED (Figure 2(f)) does not show the signs of crystallinity. Although this confirms the influence of annealing treatment on the atomic configuration of the products, the extent of modification has been insufficient to establish any remarkable long range crystalline order. Figure 2(g, h) shows the products of calcination at 1100°C, demonstrating clear changes in the appearance of the powders. The large particles have fragmented into smaller ones (compare Figure 2(g) with Figure 2(d)) probably due to the stresses induced by genesis of crystalline phases. Moreover, the HRTEM image (Figure 2(h)) demonstrates the presence of tiny nanocrystals embedded in the matrix of the larger particles. These could be either Al_2O_3 nanoparticles crystallised at high temperature due to the presence of excess aluminium in the sol-gel precursors, or even, $AlPO_4$ crystallites emerged as isolated islands in the matrix of the amorphous–crystalline products. The SAED image of this sample (Figure 2(i)) clearly reveals crystalline rings and spots demonstrating the presence of both Al_2O_3 and $AlPO_4$ according to the XRD pattern presented in Figure 1(c).

FTIR investigations

The FTIR spectra of the synthesised non-stoichiometric amorphous aluminium phosphate (Al:P = 1.75:1) is shown in Figure 3. The main characteristic peaks of aluminium phosphate are related to the phosphate agent groups (PO_4^{3-}) and Al−O−P bonding. These characteristic peaks are attributed to the Al−O−P bending mode at 970 cm^{-1}, the Al−O−P stretch at 1120 cm^{-1} and its rocking mode at 580 cm^{-1}. Moreover, the peaks appeared at 1716 and 1038 cm^{-1} are assigned to the P-OC_2H_5 ester groups indicating polyesterification reactions done during the sol-gel synthesising process [10,11].

The bands related to the characteristic peaks of hydroxyl group (OH^-) appear in 1450 and 1640 cm^{-1}. It is suspected that the source of water is from the water of hydration presented in the aluminium nitrate added to the precursor. It is notable that the OH^- bending vibration appears near 1640 cm^{-1} and is considerably weaker than the OH^- stretching modes [10,12].

The sharp peak at 1382 cm^{-1} is related to the P=O stretch vibrations, while it is not observed in the berlinite spectrum. This peak has observed in a variety of phosphate glasses. However, the P=O as a terminal group, does not appear in crystalline aluminium phosphates. The P=O is known to be a constituent in phosphate glasses that disrupts the crystalline network. This band appears very similar to those in the spectra of binary phosphosilicate glasses [13].

Another different feature in the FTIR spectra of the crystalline and amorphous aluminium phosphate is the presence of a peak at 830 cm^{-1} in the amorphous aluminium phosphate spectrum, unlike the crystalline one. This is related to the Al−O−Al bonds caused by excess aluminium content in the precursor solution present beyond the Al:P = 1:1 molar ratio in the stoichiometric $AlPO_4$ composition. The intensity of this band increases with increasing the aluminium content and can be assigned to Al–O–Al stretching [14]. It is worth mentioning that the presence of such 'interrupting' Al–O–Al groups in a continuous network containing Al–O–P linkages resist the nucleation of both crystalline $AlPO_4$ and Al_2O_3, and thus retaining the amorphous character

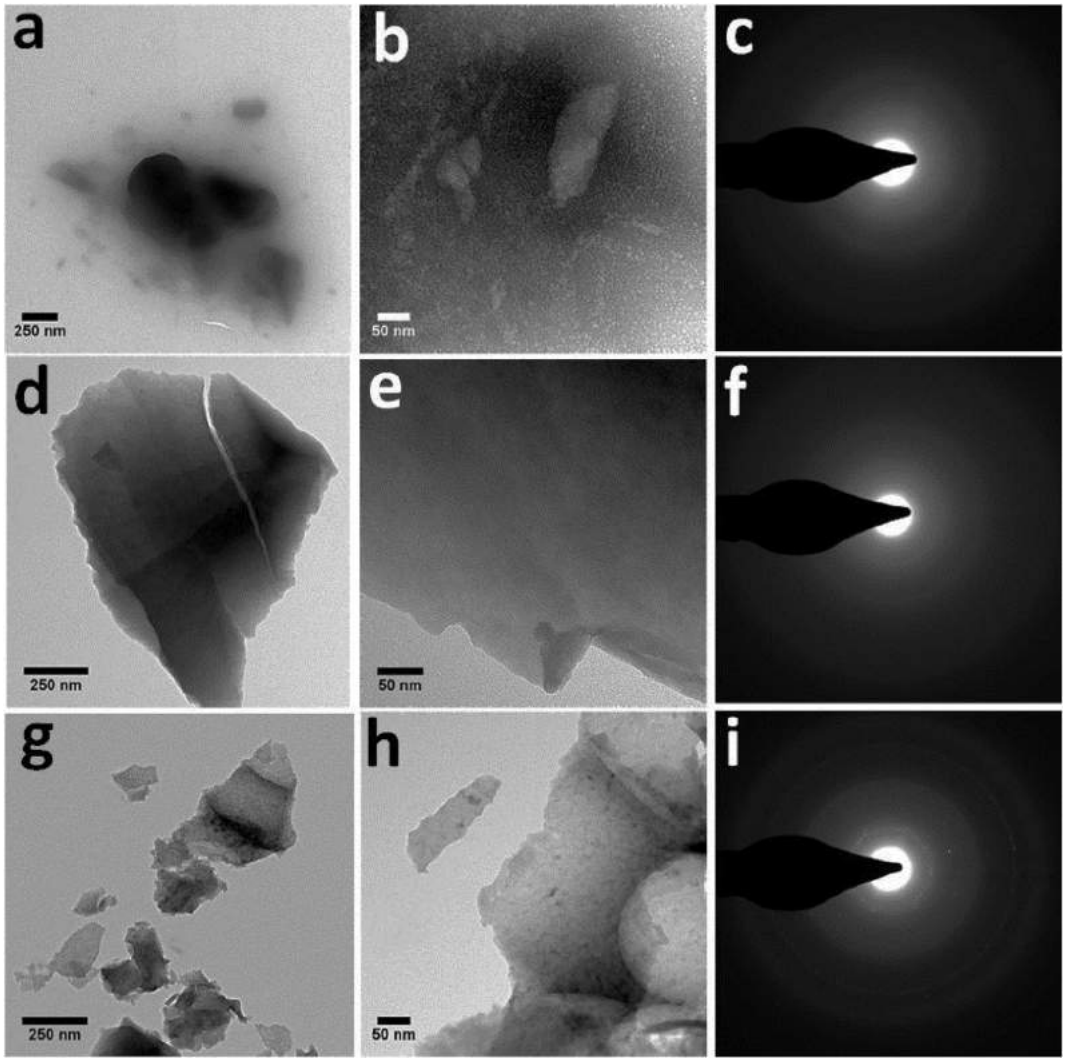

Figure 2. (a) TEM, (b) HRTEM and (c) SAED of aluminium phosphate gel dried at 65°C, (d) TEM, (e) HRTEM and (f) SAED of aluminium phosphate powder annealed at 500°C for 15 min, (g) TEM, (h) HRTEM and (i) SAED of aluminium phosphate powder calcined at 1100°C for 1 h.

to elevated temperatures. It is expected that the thermal stability is extended to higher temperatures with increasing the amount of excess aluminium in the precursor solution.

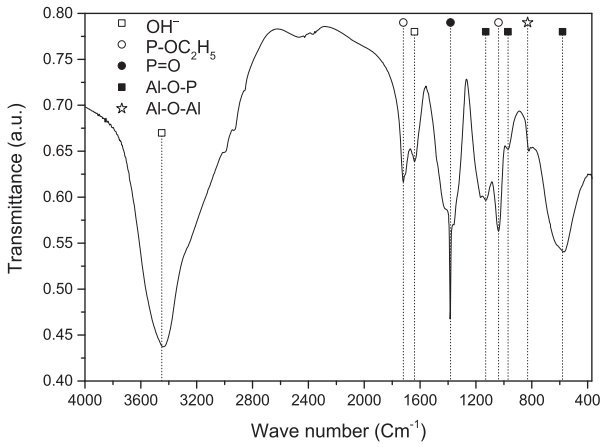

Figure 3. FTIR spectra of the synthesised non-stoichiometric amorphous aluminium phosphate (Al:P = 1.75:1).

Cyclic oxidation resistance

Figure 4 represents the measured weight changes per unit area of the bare stainless steel 304 and aluminium phosphate coated substrate plotted against the

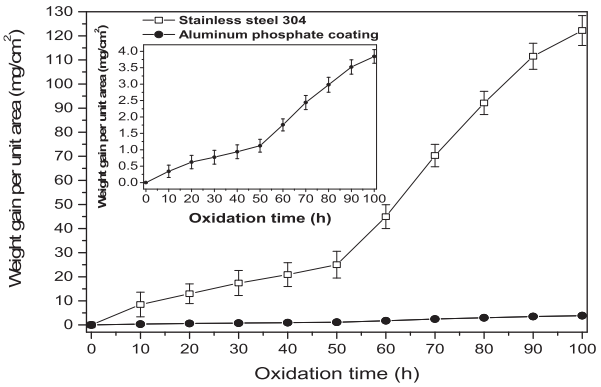

Figure 4. Weight gain per unit area vs. oxidation time for AISI 304 stainless steel and aluminium phosphate coating (inset: weight change per unit area of aluminium phosphate coating vs. oxidation time).

oxidation time. The weight change of the coated substrate against the oxidation time is separately plotted as an inset for more clear demonstration of oxidation law of the coating material.

It is evident from Figure 4 that the weight gain of the coated sample after 100 h exposure to the air at 1100°C (4 mg cm^{-2}) is remarkably lower than the bare one (120 mg cm^{-2}), signifying the protective effect of the applied aluminium phosphate coating due to retarding the inward-diffusion of oxygen and outward-diffusion of iron [15]. It is also observed that both coated and uncoated surfaces follow a similar trend of weight gain during the cyclic oxidation process, although the coating has a major kinetic effect and retards the scale spalling, as the obtained weight gain of the bare substrate was almost 30 times greater than that of the coated sample.

Figure 5 represents the XRD patterns of the oxidised bare and aluminium phosphate coated substrates after exposure to the air at 1100°C for 100 h. The protective effect of aluminium phosphate coating against high temperature oxidation could be realised in comparison between the coated and uncoated samples, where the oxide peaks and their intensity have remarkably decreased in the coated sample. Such a capability is attributed to the low oxygen diffusivity of the synthesised amorphous aluminium phosphate. Comparing to the bare substrate, the spinel oxide $FeCr_2O_4$ (ICDD Card No. 34-0140) peaks are dominant in coated sample, indicating the more oxidation resistance of the coated substrate than the bare one. It is notable that the spinel oxides are complex compounds which prevent diffusion of metal cations and oxygen ion through the oxide layer, and thus, decelerate the oxidation rate [16].

It should be pointed out that the oxidised bare substrate is mainly consisted of Fe_2O_3 (ICDD Card No. 33-0664) indicating the chromium depletion of the substrate/oxide interface by alternate formation and spallation of Cr-rich spinel oxide ($FeCr_2O_4$) on the surface [17]. It means that there is not sufficient chromium

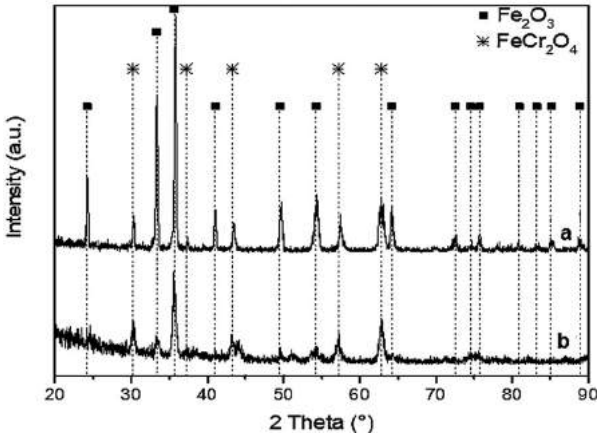

Figure 5. XRD patterns of (a) bare AISI 304 stainless steel substrate and (b) aluminium phosphate coated substrate after oxidation at 1100°C for 100 h.

content to form the protective chromium oxide film on the surface, which leads to nucleation of non-protective Fe-rich oxide, and results in increase of the oxidation rate [18]. This behaviour was further confirmed by weight gain plots and cross-sectional studies.

Figure 6 demonstrates the microstructure and EDS maps of the cross-section of bare stainless steel 304 after oxidation at 1100°C for 10 h and the aluminium phosphate coated substrate after oxidation at 1100°C for 10 and 100 h. It should be noted that after 100 h of thermal cyclic oxidation, the bare substrate completely failed due to alternate formation and spalling of the oxide scales, somehow that the cross-sectional study was not possible.

The thickness of the oxide layer formed on the surface of the bare substrate after 10 h oxidation is estimated 50 μm, while it is around 6 and 11 μm for the coated surface after 10 and 100 h of the cyclic oxidation, respectively.

The presence of iron, chromium and oxygen in the oxide layer formed on the bare and coated surfaces are clearly observed in the EDS maps presented in Figure 6. Moreover, there is a significant difference in the iron content of the oxide layer formed on the bare substrate after 10 h oxidation and the coated one after 10 and even 100 h exposures to the air. High concentration of iron in the oxide layer formed on the bare substrate compared to that of the coated one reveals the consumption of the un-protected metal substrate and surface protection ability of the aluminium phosphate coating during the high temperature oxidation cycles. On the other hand, according to the Cr distribution map of the bare substrate after 10 h oxidation (Figure 6(a)), it can be seen that there is a narrow region at the substrate/oxide interface with lower Cr content than the bulk metal, confirming chromium depletion. The chromium depletion phenomenon shows that the Cr content is not high enough to support the formation of a protective oxide layer on the surface against the oxidation, which leads to a Fe-rich oxide layer. However, this phenomenon could not be observed from the EDS maps of the aluminium phosphate coated surfaces (Figure 6(b,c)).

Conclusions

Non-stoichiometric and amorphous aluminium phosphate was synthesised by sol-gel process. The XRD analysis showed that the sol-gel product is completely amorphous and transforms to amorphous-nanocrystalline structure after annealing at 1100°C for 1 h. The TEM observations were further confirmed the amorphous and amorphous-nanocrystalline structures which had been already revealed by the XRD patterns. Based on the FTIR result, the non-stoichiometric amorphous aluminium phosphate owned Al−O−Al bonding besides Al−O−P groups caused by excess

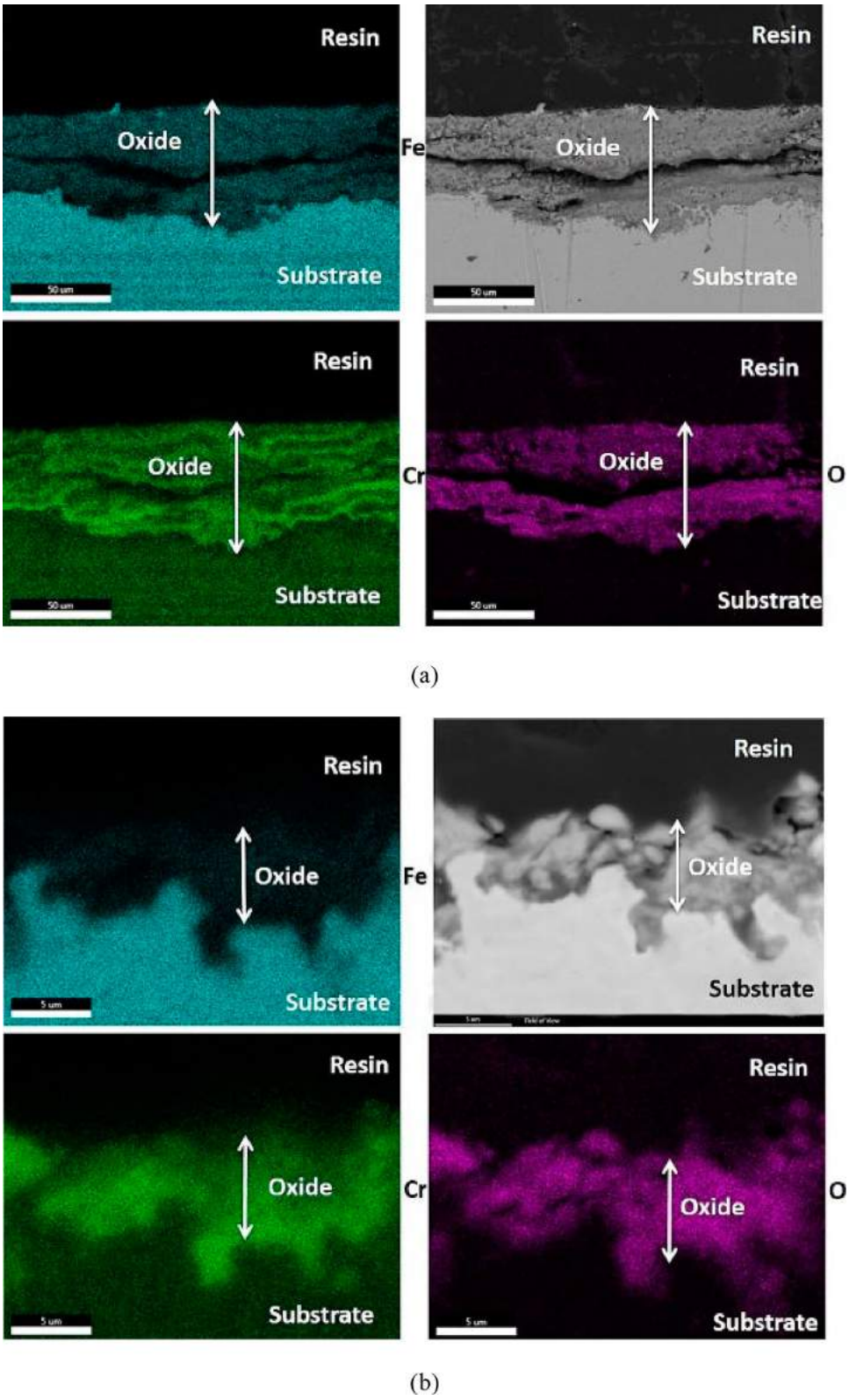

Figure 6. EDS maps of (a) AISI 304 stainless steel after oxidation at 1100°C for 10 h, (b) aluminium phosphate coating after oxidation at 1100°C for 10 h, (C) aluminium phosphate coating after oxidation at 1100°C for 100 h.

aluminium content present in the precursor solution and responsible for metastability at elevated temperatures. The weight gain measurements after 100 h oxidation test revealed that the range of the weight change of the bare substrate was 30 times greater than that of the coated one. Also, the formation of spinel oxides on the coated surface and haematite on the uncoated surface were dominant after oxidation test indicating the superior oxidation resistance of the amorphous aluminium phosphate coating.

In general, the results showed that the applied amorphous aluminium phosphate coating could successfully provide surface protection of stainless steel against degradation over 1000°C.

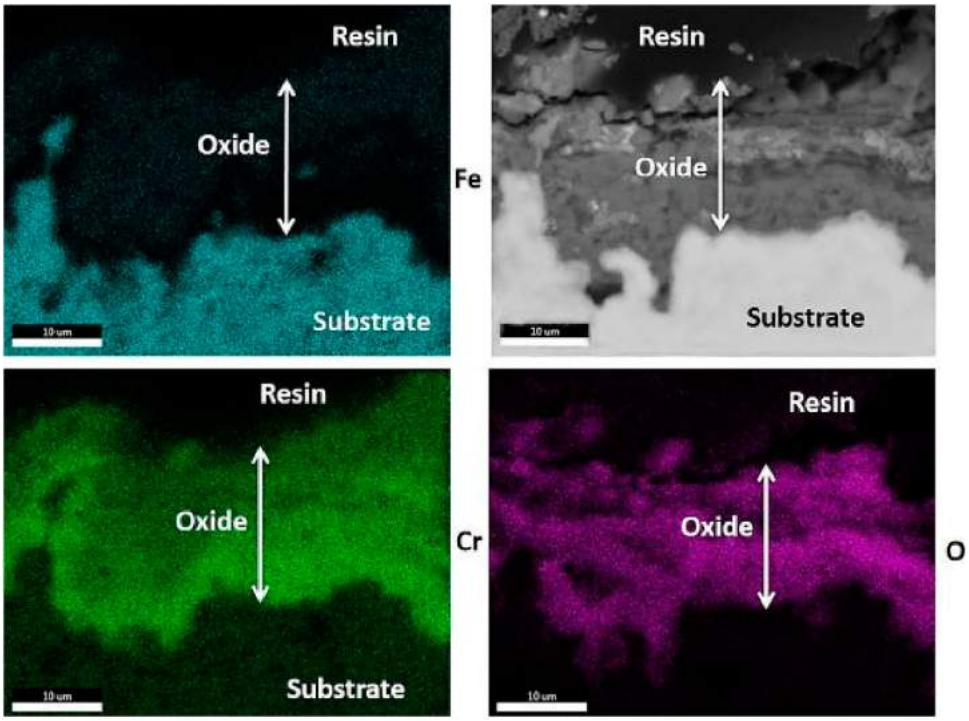

Figure 6. Continued.

Acknowledgement

The authors greatly appreciate the generous support of Department of Chemistry, Materials and Chemical Engineering, Polytechnic University of Milan, Italy and in particular, Professor Massimiliano Bestetti on this research.

Disclosure statement

No potential conflict of interest was reported by the authors.

References

[1] Li N, Zhong M, Zh X, et al. Polyesterification synthesis of amorphous aluminum phosphate thermal radiation material with high infrared emissivity. Mater Lett. 2018;213:335–337.
[2] Chen D, He L, Sh S. Study on aluminum phosphate binder and related Al_2O_3-SiC ceramic coating. Mater Sci Eng A. 2003;348:29–35.
[3] Xu R, Pang W, Yu J, et al. Chemistry of zeolites and related porous materials: synthesis and structure. Singapore: John Wiley & Sons; 2007.
[4] Stachurski ZH. On structure and properties of amorphous materials. Materials. 2011;4:1564–1598.
[5] Devamani RHP, Alagar M. Synthesis and characterization of aluminum phosphate nanoparticles. Int J Appl Sci Eng Res. 2012;1:769–775.
[6] Onoda H, Fukumura Y, Takenaka A. Preparation of POROUS aluminum phosphate with various acidic and basic compounds. J Mat Sci Eng Adv Technol. 2010;1:97–108.
[7] Campelo JM, Jaraba M, Luna D, et al. Effect of phosphate precursor and organic additives on the structural and catalytic properties of amorphous mesoporous $AlPO_4$ materials. Chem Mater. 2003;15:3352–3364.
[8] Liu G, Jia M, Zh Z, et al. Synthesis and pore formation study of amorphous mesoporous aluminophosphates in the presence of citric acid. J Colloid Interface Sci. 2006;302:278–286.
[9] Niederberger M. Nonaqueous sol-gel routes to metal oxide nanoparticles. Acc Chem Res. 2007;40:793–800.
[10] Sun DL, Deng JR, Chao Z. Catalysis over zinc-incorporated berlinite ($ZnAlPO_4$) of the methoxycarbonylation of 1,6-hexanediamine with dimethyl carbonate to form dimethylhexane-1,6-dicarbamate. Chem Cent J. 2007;1:1–9.
[11] Wiliana Y, Li T, Tam KC. Synthesis of amorphous calcium phosphate using various types of cyclodextrins. Mater Res Bull. 2007;42:820–827.
[12] Priya SS, Kumar VP, Kantam ML, et al. Catalytic performance of $Pt/AlPO_4$ catalysts for selective hydrogenolysis of glycerol to 1,3-propanediol in the vapor phase. RSC Adv. 2014;4:51893–51903.
[13] Muraoka Y, Kihara K. The temperature dependence of the crystal structure of berlinite, a quartz-type form of $AlPO_4$. Phys Chem Mineral. 1997;24:243–253.
[14] Ortiz A, Alonso JC, Pankov V, et al. Characterization of amorphous aluminum oxide films prepared by the pyrosol process. Thin Solid Films. 2000;368:74–79.
[15] Luo L, Yao J, Li J, et al. Preparation and characterization of sol–gel Al_2O_3/Ni–P composite coatings on carbon steel. Ceram Int. 2009;35:2741–2745.
[16] Birks N, Meier GH, Pettit FS. Introduction to the high temperature oxidation of metals. 2nd ed. New York (NY): Cambridge University; 2006.
[17] Huntz AM, Reckmann A, Haut C, et al. Oxidation of AISI 304 and AISI 439 stainless steels. Mater Sci Eng A. 2007;447:266–276.
[18] Wei DB, Huang JX, Zhang AW, et al. Study on the oxidation of stainless steels 304 and 304L in humid air and the friction during hot rolling. Wear. 2009;267:1741–1745.